High-resolution total-cross-section measurements for electron scattering from Ar, Kr, and Xe employing a threshold-photoelectron source

M. Kurokawa,[1,*] M. Kitajima,[1,†] K. Toyoshima,[1] T. Kishino,[1] T. Odagiri,[1] H. Kato,[2] M. Hoshino,[2] H. Tanaka,[2] and K. Ito[3]

[1]*Department of Chemistry, Tokyo Institute of Technology, Tokyo 152-8551, Japan*

[2]*Department of Physics, Sophia University, Tokyo 102-8554, Japan*

[3]*Photon Factory, Institute of Materials Structure Science, Tsukuba 305-0801, Japan*

(Received 25 October 2011; published 29 December 2011)

Absolute total cross sections for electron scattering from Ar and Xe at electron energies ranging from 7 meV to 20 eV were obtained with the experimental technique employing the threshold-photoelectron source. The measured total cross sections are in good agreement with those obtained by other groups down to 100 meV, above which several experimental works have been reported. Scattering lengths for electron scattering from Ar, Kr, and Xe were determined from the present total cross sections and our recent results for Kr using the modified effective range theory. The values of the scattering length obtained in the present analysis differ from the values determined from the previous swarm experiments and beam experiments. The resonant structures in the total cross sections due to Feshbach resonances of Ar, Kr, and Xe with an improved energy resolution were also measured. Analyses of the resonant structure were carried out based on the spin-dependent resonant scattering theory in order to determine the values of the natural width of Feshbach resonances of Ar, Kr, and Xe precisely.

DOI: 10.1103/PhysRevA.84.062717 PACS number(s): 34.80.Bm, 52.20.Fs

I. INTRODUCTION

The scattering of low-energy electrons by rare-gas atoms has been the subject of extensive experimental and theoretical investigations. Accurate absolute cross sections for electron scattering from heavier rare-gas atoms, such as Ar, Kr, and Xe, provide a critical test of the various theoretical models, including correlation-polarization interactions and relativistic effects in electron collision. Reliable cross-section data for electron scattering from rare-gas atoms are also of crucial importance in applications, such as electron-driven processes in phenomena of the earth and the planets, radiation chemistry, gaseous discharges, plasmas, and so on.

Among the measurable cross sections for various scattering processes, the grand total cross section is one of the most reliable quantities since it can be determined without any normalization procedure. The measured absolute values offer the upper bound of the scattering cross section comprising the elastic as well as all of the inelastic scattering, including attachment processes. The total-cross-section curves for electron scattering from Ar, Kr, and Xe are characterized by a maximum at around 5–10 eV, and the well-known Ramsauer-Townsend minimum [1,2] below 1 eV. Each cross-section curve shows a steep rise with a decrease of the electron energy below the Ramsauer-Townsend minimum, and the determination of the cross sections at the zero-energy limit has been the subject of many studies [3–10], though the lowest energy of the measurements has been limited to about 100 meV.

The standard experimental technique, using a hot filament electron source followed by an electrostatic monochromator, delivers a typical electron-energy width of 30–150 meV and the lower energy limit is about 100–250 meV. Another technique using time-of-flight energy selection with pulsed electron beams has been proposed [7–9], which gives energy-dependent resolution of as high as 5 meV at low incident energies (>250 meV). An alternative method for reaching higher resolutions is through near-threshold photoionization of atoms by making use of a photoelectron source, as realized by Gallagher and York [11,12]. By making use of a photoelectron source together with high-resolution synchrotron radiation, Field and Ziesel and co-workers succeeded in the measurement of the total cross section for electron scattering from various molecules below 100 meV, where collisions become essentially in the cold regime in which the de Broglie wavelength of the incident electrons is very much greater than the range at which there is significant interaction between the electron and the atom or molecule [13,14]. However, measurements of the total cross section for electron scattering from Ar, Kr, and Xe using this technique have not been reported.

Electron-swarm techniques have also been used to derive cross-section data, such as momentum-transfer cross sections, for rare-gas atoms at very low energy [15–23]. The method provided the information over an energy range from about 10 meV to a few eV, which has been very difficult to access by the standard single-collision experiments. However, since the microscopic properties have to be determined in a complicated unfolding procedure by a self-consistent set of cross sections that will reproduce the macroscopic experimental results such as transport coefficients, drift velocity, or mobility via the solution of the energy distribution function, which often is of the non-Maxwellian form, difficulty arises in determining the accurate cross section uniquely by the swarm techniques [22,24].

Recently, we developed a method for producing an electron beam at very low energy for a cold electron collision experiment employing the threshold-photoelectron source [25]. The technique enables one to perform high-energy resolution experiments at very low electron energies by employing the penetrating-field technique together with the threshold photoionization of atoms by the synchrotron radiation. The

*Present address: Central Research Laboratory, Hitachi Ltd., Tokyo 185-8601, Japan.

†mkitajim@chem.titech.ac.jp

total cross sections for electron scattering from Kr in the energy range from 14 meV to 20 eV were obtained at an electron-energy width of 11 meV with the apparatus employing the threshold-photoelectron source. In addition, the resonant structures in the total cross sections due to the Kr^- $(4p^5 5s^2\,{}^2P_{3/2})$ and the Kr^- $(4p^5 5s^2\,{}^2P_{1/2})$ Feshbach resonances were also obtained and reported.

Here we present the results of the measurements of total cross sections for electron scattering from Ar and Xe obtained by the experimental technique employing the threshold-photoelectron source in the energy range from 20 eV down to 7 meV. Scattering lengths for electron scattering from Ar, Kr, and Xe were determined from the total cross sections obtained in the present measurements and those reported in our recent work [25] using the modified effective range theory (MERT) [3,10,26,27].

We also report on the total cross sections around the Feshbach resonances of Ar, Kr, and Xe with an improved energy resolution. The resonant structure of the Feshbach resonances for electron scattering from these rare-gas atoms have been studied extensively by transmission measurements [28–30] and elastic electron-scattering measurements [31–36]. However, the total cross sections for these resonances have not been reported except for Kr [25].

II. EXPERIMENT

The present measurements were carried out at beam line 20A of the Photon Factory at Japan's National Laboratory for High Energy Physics (KEK), using an electron-scattering apparatus equipped with a threshold-photoelectron source [25]. Briefly, threshold photoelectrons produced by the threshold photoionization of Ar atoms are extracted from the photoionization cell by a very weak electrostatic field, typically an electric field of about 0.02 V/cm in the center of the photoionization region, formed by the penetrating-field technique. The ionizing photon beam is the monochromatized synchrotron radiation tuned just at the first ionization potential of Ar (15.760 eV) from the 3 m normal-incidence monochromator equipped at beam line 20A [37]. The extracted electrons are formed into a beam by the first electron lens systems and transferred to the collision cell filled with the target gas. The electrons passing through the cell without any collision with the target are angular discriminated and refocused by the third lens system and detected by a channel electron multiplier. The counting rates of the detected electrons in the presence and absence of the target gas are converted to the total cross section for electron scattering according to the attenuation law. The typical counting rate of the electrons was 10 000 cps at electron energy of 100 meV. A cross section of the electron-scattering apparatus is shown in Fig. 1.

The penetrating field forms a saddle point in the potential distribution that has the effect of focusing and enhancing the extraction efficiency of photoelectrons of the particular energy. By tuning the penetrating field, only very-low-energy photoelectrons can be extracted from the photoionization region and focused onto the entrance of the lens system, while the energetic photoelectrons rapidly diverge [38]. This effect results in a very narrow energy width of the electron beam from the threshold-photoelectron source, even if the bandwidth

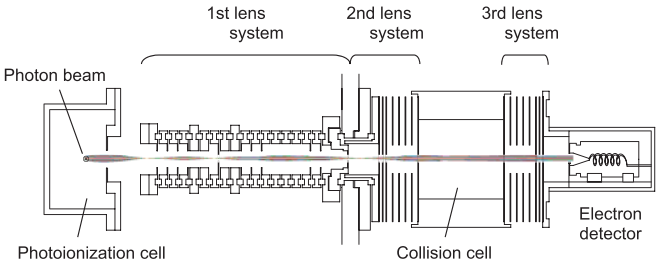

FIG. 1. (Color online) Cross section of the apparatus used in the present measurements. The photoionization cell and the first electrostatic lens system serve as the threshold-photoelectron source. A monochromatic photon beam at the first ionization threshold of Ar (15.760 eV) is introduced into the photoionization cell. The photoelectrons are collected by the penetrating field from the first lens system and formed into a beam. The energy of the electron beam is tuned by the second lens system and focused onto the collision cell filled with the target gas. The transmitted electrons are angular discriminated and refocused by the third lens system and detected by a channel electron multiplier. The results of the electron trajectory calculation at the collision energy of 0.1 eV are also shown.

of the ionization photon beam is fairly wide [25]. Doppler broadening of the threshold photoelectrons is very small in the present case. The energy broadening due to the Doppler effect is estimated to be less than 0.1 meV.

The whole of the photoionization cell and scattering apparatus are placed inside the double μ-metal shields to attenuate the earth's magnetic field. The stray magnetic field is estimated to be less than 10^{-7} T, which is sufficiently small not to interact with the lowest energy electron in the present experiment.

The total cross section was obtained by using the attenuation law,

$$I(E) = I_0(E)\exp[-\sigma(E)nL], \tag{1}$$

where $I(E)$ and $I_0(E)$ are attenuated and unattenuated electron intensities obtained at the impact energy E, respectively, $\sigma(E)$ is the total cross section, n is the number density of the target gas, and L is the effective path length of the electron in the target gas, which has been found to be equal to the geometrical length [25]. In the present experiment, the transmission of the electron beam (I/I_0) was kept above 50% in order to avoid inaccurate measurements for a narrow structure, known as the line saturation effect [39].

The pressure of the target gas was measured by a capacitance manometer kept at a temperature of 318 K and the thermal transpiration correction with the empirical expression developed by Takaishi and Sensui [40] was made in the present measurement. The purity of the gases in the present measurements was 99.9995% for Ar and 99.99% for Kr and Xe.

In the attenuation method, the effect of the forward scattering, that is, incomplete discrimination against the electrons scattered at small angles with forward direction due to the finite angular resolution, contributes to the measured total cross section. In the present study, the contributions from the forward-scattered electrons of the scattering from Ar and Xe were estimated by the same manner described in Ref. [25]. The CPO computer program [41] was used to calculate the

trajectory of the electrons scattered in the collision cell, and the theoretical phase shifts reported by McEachran and Stauffer [42,43] were applied in order to estimate the differential cross sections for the electron scattering from Ar and Xe. As was the case for Kr [25], it was found that the contribution from the forward-scattered electron is negligible in the present study. The use of the independent third lens system enables accurate discrimination against the forward-scattered electrons in a wide energy range, from the energy region of a few milli-electron volts to a few tenths of electron volts.

The stability of the photon beam intensity was achieved by the top-up operation of the Photon Factory facility that has been available in the recent operation [44]. Since the instability of the energy of the photon beam at a narrow photon bandwidth causes fluctuation in the electron-beam intensity, we have used a lower resolution of about 4 meV for the photon beam during the measurement. The size of the photon beam was 1 mm in diameter.

The energy and the width of the electron beam were estimated by fitting the theoretical cross sections convoluted with a Gaussian function representing the resolution to those measured at around the Feshbach resonances of each rare-gas atom. The energy of 11.1030 ± 0.0010 eV [35] for the resonance energy of the Ar^- $(3p^5 4s^2\,{}^2P_{3/2})$ resonance and that of 7.901 ± 0.016 eV [34] for the Xe^- $(5p^5 6s^2\,{}^2P_{3/2})$ resonance were chosen as the reference point. The accuracies of the energy scale of the present measurements were estimated to be ± 3 meV for Ar and ± 16 meV for Xe. The energy widths of the electron beam for the total-cross-section measurement at 7 meV to 20 eV were estimated to be 10 meV for Ar and 12 meV for Xe.

In the present study, we also measured the total cross sections from electron scattering from Ar, Kr, and Xe at around the Feshbach resonances of each atom with an improved energy resolution. The improvement of the resolution was achieved by reconstructing the collision cell by changing its material from stainless steel to molybdenum. In this high-resolution measurement, energy widths of the electron beam were estimated to be 8.4, 7.0, and 8.6 meV for Ar, Kr, and Xe, respectively.

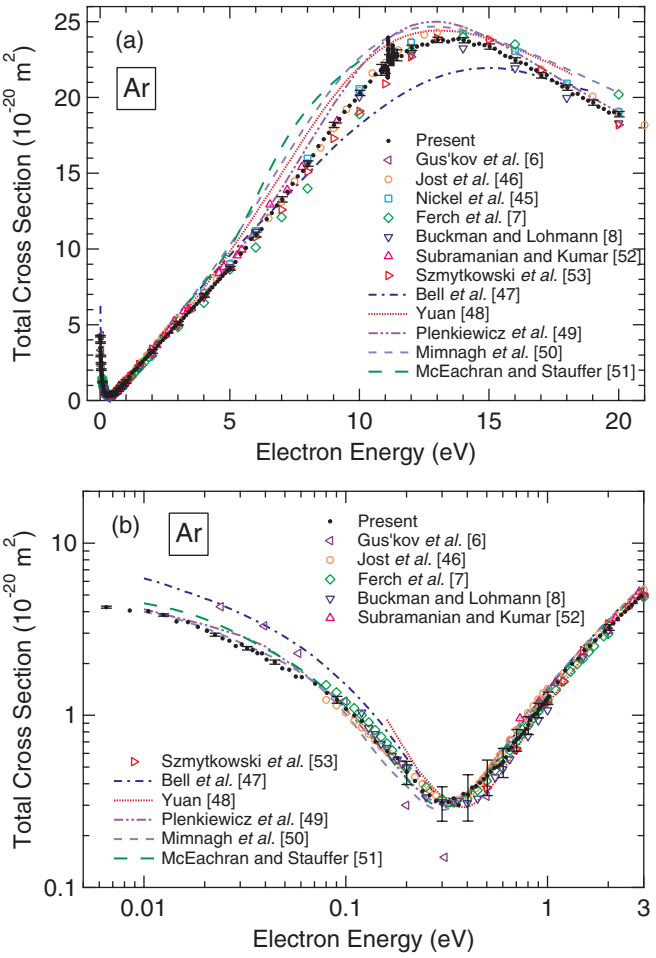

FIG. 2. (Color online) Total cross section for electron scattering from Ar (a) in the energy range up to 20 eV, and (b) in the energy range below 3 eV; • indicates the present results. Also shown are experimental results of Gus'kov *et al.* [6], ◁; Jost *et al.* [46], ○; Nickel *et al.* [45], □; Ferch *et al.* [7], ◇; Buckman and Lohmann [8], ▽; Subramanian and Kumar [52], △; and Szmytkowski *et al.* [53], ▷; and theoretical results of Bell *et al.* [47], – · –; Yuan [48], · · · ; Plenkiewicz *et al.* [49], – · · · –; Mimnagh *et al.* [50], – –; and McEachran and Stauffer [51], — —.

III. RESULTS AND DISCUSSION

A. Total cross section for electron scattering from Ar and Xe in the energy range from 7 meV to 20 eV

The total cross sections for electron scattering from Ar obtained in the energy range of 7 meV to 20 eV in the present experiment are shown in Fig. 2(a). The numerical values for the selected points are also shown in Table I. The overall uncertainty in the cross section includes the statistical and systematic error. In Fig. 2(a), the well-known Ramsauer-Townsend minimum is seen at around 0.3 eV and the cross section rises gradually, reaching a maximum around 14 eV, and then decreases slowly with increasing electron energy. The position of the Ramsauer-Townsend minimum obtained from the MERT fit described in the next section was 0.338 ± 0.005 eV. At around 11 eV, the very sharp structures due to the Ar^- $(3p^5 4s^2\,{}^3P_{3/2}, {}^3P_{1/2})$ Feshbach resonances are also seen on the present total-cross-section curve. Below the Ramsauer-Townsend minimum, the cross section increases rapidly with decreasing electron energy.

Previous experimental and theoretical cross sections are also shown for comparison in Fig. 2(a). In general, the present results agree with the reported experimental data. In the energy region above 4 eV, the present cross sections agree very well with those obtained by Nickel *et al.* [45].

In Fig. 2(b), a comparison of the total cross sections for electron scattering from Ar obtained in the present study with previously reported results is made in the energy range below 3 eV. The present cross-section curve agrees with those of Jost *et al.* [46], Ferch *et al.* [7], and Buckman and Lohmann [8], down to ∼100 meV within the experimental errors. At energies below ∼100 meV, cross sections obtained by Gus'kov *et al.* [6], which show a large discrepancy from other previous results around the Ramsauer-Townsend minimum, are the only available data in the literature. The present results show a large

TABLE I. The values of the total cross sections for electron scattering from Ar and Xe obtained in the present work [here and Table IV, the quoted uncertainties in parentheses refer to the respective last digits—e.g., 18.90(17) means 18.90 ± 0.17].

Energy (eV)	$\sigma(E)$ (10^{-20}m^2) Ar	Xe
20.02	18.90(17)	34.72(47)
19.02	19.66(17)	35.21(47)
18.02	20.65(18)	35.54(47)
17.02	21.46(18)	35.61(47)
16.02	22.45(18)	35.98(47)
15.02	23.37(18)	36.18(47)
14.02	23.78(18)	36.66(47)
13.02	23.80(18)	36.98(47)
12.02	23.28(17)	37.47(47)
11.02	22.00(36)	38.26(47)
10.02	20.30(17)	39.29(47)
9.02	18.18(17)	40.40(44)
8.02	15.64(17)	41.17(38)
7.02	13.27(17)	41.64(47)
6.02	10.95(17)	40.84(47)
5.02	8.73(12)	37.07(33)
4.52	7.86(12)	33.76(33)
4.02	6.94(12)	29.21(33)
3.52	6.05(12)	24.16(33)
3.02	5.10(12)	18.80(16)
2.52	4.20(12)	13.76(16)
2.32		11.83(16)
2.12		9.95(16)
2.02	3.24(12)	
1.933		8.30(24)
1.853		7.61(24)
1.823	2.90(12)	
1.773		6.95(24)
1.693		6.46(24)
1.623	2.54(12)	
1.613		5.95(24)
1.533		5.25(24)
1.453		4.74(24)
1.423	2.13(12)	
1.373		4.14(24)
1.293		3.69(24)
1.223	1.82(12)	
1.213		3.20(24)
1.133		2.67(24)
1.123	1.55(12)	
1.053		2.43(24)
1.023	1.29(10)	
1.013		2.10(24)
0.973		2.09(24)
0.933		1.94(24)
0.923	1.11(10)	
0.893		1.80(24)
0.853		1.67(24)
0.823	0.94(10)	
0.813		1.73(24)
0.773		1.58(24)
0.733		1.60(24)
0.723	0.74(10)	
0.693		1.76(24)
0.653		1.69(24)
0.623	0.57(10)	
0.613		1.86(24)
0.573		2.11(24)
0.533		2.30(24)
0.523	0.47(10)	
0.493		2.51(24)
0.483	0.43(10)	
0.453		3.13(24)
0.443	0.39(10)	
0.413		3.75(24)
0.403	0.35(10)	
0.383	0.35(10)	
0.373		4.31(24)
0.363	0.30(10)	
0.343	0.33(10)	
0.333		5.42(24)
0.323	0.31(10)	
0.301	0.31(7)	
0.293		6.74(24)
0.281	0.32(7)	
0.261	0.34(7)	
0.253		8.47(24)
0.241	0.36(7)	
0.221	0.42(7)	
0.213		10.87(24)
0.201	0.47(7)	
0.181	0.56(7)	
0.173		14.13(37)
0.161	0.62(7)	15.05(37)
0.141	0.70(7)	17.77(38)
0.121	0.93(6)	20.88(38)
0.111	1.00(6)	22.48(38)
0.101	1.09(6)	24.44(38)
0.091	1.23(6)	27.19(39)
0.081	1.35(6)	29.81(39)
0.071	1.53(6)	32.65(40)
0.061	1.67(6)	36.55(42)
0.057	1.68(6)	37.97(43)
0.053	1.84(6)	39.40(45)
0.049	1.87(6)	41.41(46)
0.045	2.04(6)	43.50(49)
0.041	2.11(6)	45.14(51)
0.037	2.29(6)	47.38(55)
0.033	2.46(6)	49.32(58)
0.029	2.53(6)	52.23(63)
0.027	2.71(6)	52.49(66)
0.025	2.80(6)	54.71(69)
0.023	2.94(6)	55.95(73)
0.021	3.10(6)	57.67(77)
0.019	3.26(6)	58.78(81)
0.017	3.47(6)	61.30(86)
0.015	3.51(6)	61.68(90)
0.013	3.82(6)	63.47(95)
0.011	4.02(6)	65.15(101)
0.009	4.06(6)	67.03(107)
0.007	4.24(6)	68.36(114)

discrepancy from the values reported by Gus'kov *et al.* [6] in the low-energy region, as was the case for Kr [25].

In comparison with the theoretical cross sections, the nonrelativistic *R*-matrix calculation of Bell *et al.* [47] shows discrepancies at very low energies below the Ramsauer-Townsend minimum, although it reproduces the position and the magnitude of the Ramsauer-Townsend minimum. A modified exchange calculation including the correlation-polarization potential of Yuan [48] generally agrees with the experimental results, except for the position of the Ramsauer-Townsend minimum, which appears at slightly higher energy. The results of the pseudopotential calculation of Plenkiewicz *et al.* [49] show excellent agreement down to very low energies, including the position and the magnitude of the Ramsauer-Townsend minimum. The calculation of Mimnagh *et al.* [50] employing the polarized-orbital approximation with a dynamic distortion effect also shows excellent agreement with the present results at the energy region below 100 meV. However, a slight shift of the position of the Ramsauer-Townsend minimum to the lower energies compared to the present cross-section curve is seen in their calculation. A relativistic version of the calculation of Mimnagh *et al.* [50] has been carried out by McEachran and Stauffer [51]. The position of the Ramsauer-Townsend minimum of their results shows good agreement with the present results, however, a slight deviation of the cross-section curve from the present results is seen at energies below 100 meV.

Figure 3(a) shows the total cross sections for electron scattering from Xe obtained in the energy range of 7 meV to 20 eV in the present experiment. The numerical values for the selected points are also shown in Table I. The Ramsauer-Townsend minimum is seen at around 0.8 eV and the cross-section maximum appears at about 7 eV for Xe. The position of the Ramsauer-Townsend minimum obtained from the MERT fit described in the next section was 0.78 ± 0.02 eV. The very sharp structures due to the Xe^- $(5p^6 6s^2\ ^3P_{3/2})$ Feshbach resonance can be seen at about 8 eV in Fig. 3(a). Below the Ramsauer-Townsend minimum, a steep rise of the cross section reaches to about 70×10^{-20} m^2 with decreasing electron energy down to 7 meV.

In comparison with the previous experimental total cross sections shown in Fig. 3(a), the present results agree well with those by Nickel *et al.* [45] and those by Szmytkowski *et al.* [53] in the energy region of 10–20 eV. Below 10 eV, our data agree very well with the results of Ferch *et al.* [54] down to the energy of the Ramsauer-Townsend minimum.

Figure 3(b) shows the comparison of the total cross sections for electron scattering from Xe obtained in the present study with the previously reported results in the energy range below 3 eV. The present cross sections generally agree with those reported by Ferch *et al.* [54] down to the Ramsauer-Townsend minimum. Below the Ramsauer-Townsend minimum, the present cross sections generally agree with those reported by Jost *et al.* [46] down to 100 meV. The present results are much smaller than the values reported by Gus'kov *et al.* [6] in the low-energy region, again for the case of Xe.

In the case of Xe, the previously reported theoretical integral elastic cross sections shown in Fig. 3(a) generally reproduce the experimental results at energies above 1 eV, except for the calculation of McEachran and Stauffer [55].

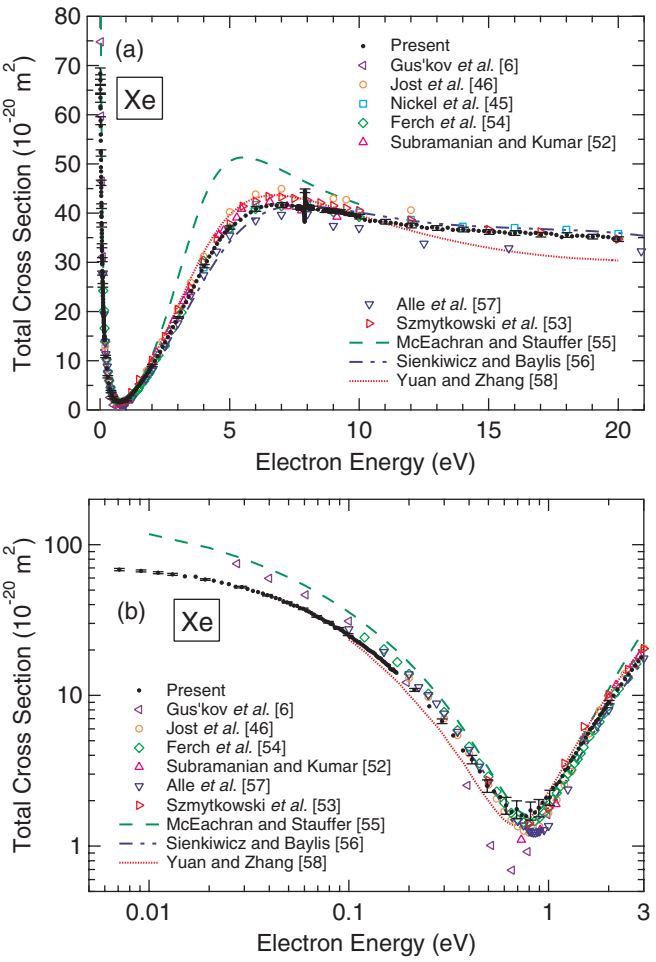

FIG. 3. (Color online) Total cross section for electron scattering from Xe (a) in the energy range up to 20 eV, and (b) in the energy range below 3 eV; • indicates the present results. Also shown are experimental results of Gus'kov *et al.* [6], ◁; Jost *et al.* [46], ○; Nickel *et al.* [45], □; Ferch *et al.* [54], ◇; Subramanian and Kumar [52], △; Alle *et al.* [57], ▽; Szmytkowski *et al.* [53], ▷; and theoretical results of McEachran and Stauffer [55], — —; Sienkiewicz and Baylis [56], – · –; and Yuan and Zhang [58], · · · .

In Fig. 3(b), the results of the relativistic calculation with a model polarization potential by Sienkiewicz and Baylis *et al.* [56] obtained above 0.4 eV agree well with the present experimental results. On the other hand, the results of the relativistic calculation by McEachran and Stauffer [55] show somewhat larger cross-section values in the very-low-energy region below the Ramsauer-Townsend minimum.

B. Scattering length for electron scattering from Ar, Kr, and Xe

Several experimental reports for the values of the scattering length, A, related to the cross section at the low-energy limit, i.e., zero-energy cross section, by $\sigma(0) = 4\pi A^2$, can be found, including both beam and swarm experiments [3–10,16,18,19,21,46,59–61]. In the present study, we have derived the scattering lengths for electron scattering from Ar, Kr, and Xe from the present total-cross-section data for Ar and Xe, and from our recent data for Kr [25], using the modified effective range theory (MERT) [3,26]. The MERT

gives analytical expressions for the scattering phase shifts as a function of the wave number of electron k, expressed in the form of the expansion of power series in k using the dipole polarizability of the target atom and four parameters, which can be determined by fitting to the scattering cross sections.

In the standard four-parameter MERT (MERT4) [3,7,10,27], phase shifts are given as

$$\tan\delta_0(k) = -Ak\left[1 + \frac{4\alpha_d k^2}{3a_0}\ln(ka_0)\right] - \frac{\pi\alpha_d k^2}{3a_0} + Dk^3 + Fk^4, \quad (2)$$

$$\tan\delta_1(k) = \frac{\pi k^2}{15a_0}\alpha_d - A_1 k^3, \quad (3)$$

$$\tan\delta_l(k) = \frac{\pi\alpha_d k^2}{a_0(2l+3)(2l+1)(2l-1)}. \quad (4)$$

Here, l is the electron angular momentum, α_d is the dipole polarizability of the atom, A is the scattering length, and D, F, and A_1 are additional fitting parameters. The total cross sections and momentum-transfer cross sections are given by the partial-wave expansions as

$$\sigma_t(k) = \frac{4\pi}{k^2}\sum_l^\infty (2l+1)\sin^2\delta_l(k), \quad (5)$$

$$\sigma_m(k) = \frac{4\pi}{k^2}\sum_l^\infty (l+1)\sin^2[\delta_l(k) - \delta_{l+1}(k)]. \quad (6)$$

We neglected the spin-orbit coupling for simplicity in this section.

The range of the validity in applying the MERT has been investigated in several reports [7,9,10,60]. Buckman and Mitroy have showed that the MERT4 is not sufficient to obtain the p-wave phase shift for an energy range above 0.5 eV for the case of Ar, and introduced an extended version of MERT with five parameters (MERT5), which enables one to obtain the phase shifts for energies up to about 1 eV [10]. In MERT5, p-wave and d-wave phase shifts have the forms

$$\tan\delta_1(k) = a_1\alpha_d k^2 - A_1 k^3 + \left(b_1\alpha_d^2 + c_1\alpha_q\right)k^4 + Hk^5, \quad (7)$$

$$\tan\delta_l(k) = a_l\alpha_d k^2 + \left(b_l\alpha_d^2 + c_l\alpha_q\right)k^4 \quad (l \geqslant 2), \quad (8)$$

where A_1, D, F, and H are fitting parameters. The effective quadrupole polarizability α_q is the difference of the static quadrupole polarizability and the nonadiabatic dipole polarizability, which is calculated from the nonadiabatic correction. The coefficients a_l, b_l, and c_l are given by

$$a_l = \frac{\pi}{(2l+3)(2l+1)(2l-1)}, \quad (9)$$

$$b_l = \frac{\pi[15(2l+1)^4 - 140(2l+1)^2 + 128]}{[(2l+3)(2l+1)(2l-1)]^3(2l+5)(2l-3)}, \quad (10)$$

$$c_l = \frac{3a_l}{(2l+5)(2l-3)}. \quad (11)$$

Buckman and Mitroy have also pointed out that the MERT5 formula describes the d-wave phase shift rather poorly in the case of electron scattering from Kr and Xe, and have introduced a further extended version of MERT with six parameters (MERT6) [10]. In MERT6, the following formula for describing the d-wave phase shift have been used:

$$\tan\delta_2(k) = a_2\alpha_d k^2 + \left(b_2\alpha_d^2 + c_2\alpha_q\right)k^4 + A_2 k^5, \quad (12)$$

where A_2 is a fitting parameter.

Figure 4(a) shows the results of the MERT5 fit to the present experimental total cross sections for electron scattering from Ar (broken curve). The fitting has been carried out in the energy range up to 1.0 eV. The values of 11.08 a_0^3 and 0.0 a_0^5, where

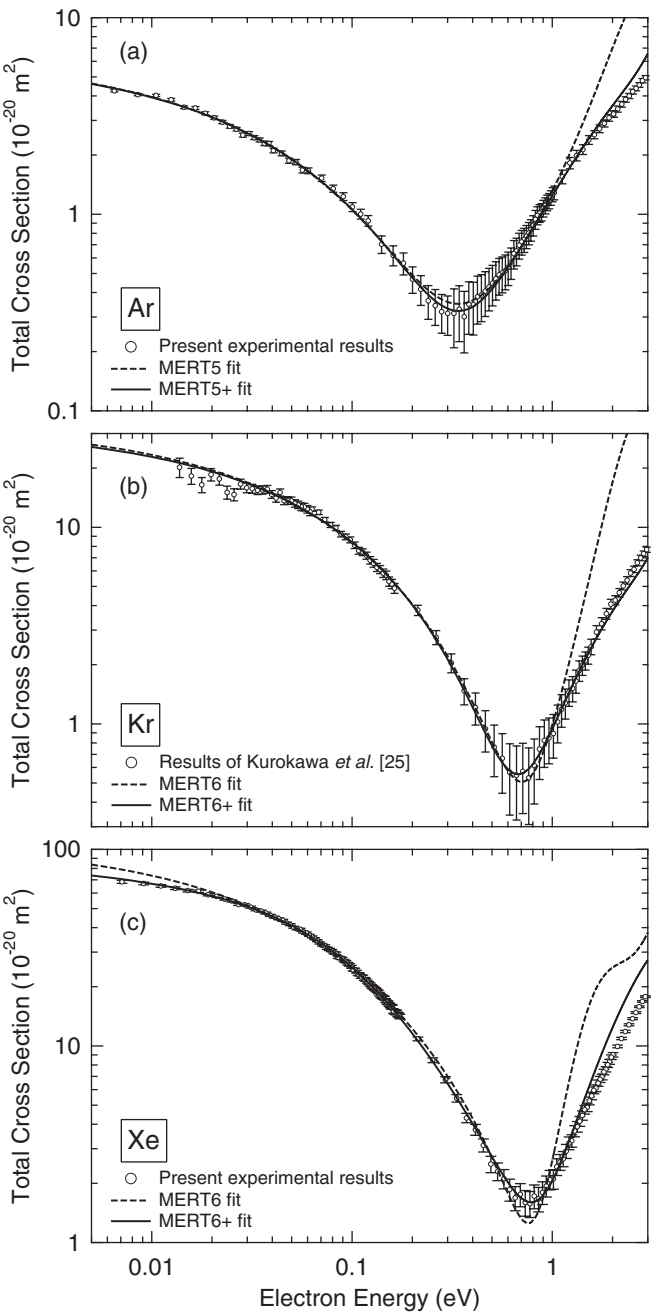

FIG. 4. Total-cross-section curves derived from the MERT fits to the experimental total cross sections for electron scattering from rare-gas atoms. (a) Ar: present experimental data, ○; MERT5 fit, - - - ; MERT5+ fit, — . (b) Kr: experimental data of Kurokawa *et al.* [25], ○; MERT6 fit, - - -; MERT6+ fit, —. (c) Xe: present experimental data, ○; MERT6 fit, - - -; MERT6+ fit, —.

a_0 is the Bohr radius, were used for the dipole polarizability α_d and effective quadrupole polarizability α_q, respectively, following Buckman and Mitroy [10]. In Fig. 4(a), the broken curve representing the MERT5 fit shows a good fit to the experimental data points within the experimental errors up to 1.0 eV.

The total-cross-section curve derived from the MERT6 fit to our recent experimental data of e^--Kr scattering [25] is shown in Fig. 4(b) as a broken curve. The fitting range was 0–1.0 eV and the values for α_d and α_q were 16.74 a_0^3 [62] and 8.0 a_0^5 [10], respectively. In Fig. 4(b), the MERT6 curve (broken curve) generally agrees well with the experimental data below 1.0 eV.

Figure 4(c) shows the results for the MERT6 fit to the present total cross sections for electron scattering from Xe, derived from the fitting range of 0–1.0 eV. Adopted values for α_d and α_q were 27.29 a_0^3 [62] and 16.8 a_0^5, respectively. The agreement of the MERT6 curve (broken curve) and experimental results becomes rather poor, especially at around the Ramsauer-Townsend minimum in the case of Xe. Also apparent is the deviation of the MERT6 fit curve from the experimental data points below about 30 meV. This deviation may cause incorrect extrapolation of the cross sections, leading to the overestimation of the absolute value of the scattering length.

In spite of its flexibility, we found that good agreement of the MERT6 fit curve between experimental data at the very-low-energy region could only be obtained when the fitting range has been limited to about 0–0.3 eV. In such case that the fitting range is limited from 0 to 0.3 eV, the MERT6 fit curve would not reproduce the magnitude of the cross section or the position of the Ramsauer-Townsend minimum. If the MERT expansion of Eq. (2) for the s-wave phase shift is valid for e^--Xe scattering, then the MERT6 curve should be able to reproduce both the cross sections at very low energy and at least the position of the Ramsauer-Townsend minimum, since both the cross sections at this very-low-energy region and the position of the Ramsauer-Townsend minimum are dominated by the s-wave phase shift. However, we found that any of the artificial MERT6 curves that follow the experimental data at very low energy below 0.1 eV would hardly reproduce the position of the Ramsauer-Townsend minimum. This shows that the s-wave phase shift derived from the MERT expansion of Eq. (2) could be used only at very low energies and becomes inadequate at energies before reaching the energy of the Ramsauer-Townsend minimum for e^--Xe scattering.

In the present study, in order to extend the valid energy region for representing the s-wave phase shift, we have expanded Eq. (2) by adding one more parameter, G, in the following form, according to O'Malley and Crompton [27]:

$$\tan\delta_0(k) = \frac{-Ak\left[1+\frac{4\alpha_d k^2}{3a_0}\ln(ka_0)\right]-\frac{\pi\alpha_d k^2}{3a_0}+Dk^3+Fk^4}{1+Gk^3}. \tag{13}$$

Equation (13) becomes identical to Eq. (2) at $k \to 0$.

An extended version of MERT6, which adopts Eq. (13) instead of Eq. (2) for the s-wave phase shift (MERT6+), was employed for fitting the experimental data. The total-cross-section curve derived from the MERT6+ fit is shown in Fig. 4(c) by a solid curve. A much better agreement was obtained for the results of the MERT6+ fit with the experimental data at the very-low-energy region and also at the energies around the Ramsauer-Townsend minimum.

The total-cross-section curve derived from the MERT6+ fit to the e^--Kr scattering is shown in Fig. 4(b) by a solid curve. In the case of Kr, although a slight modification of the fitted curve is seen at around the Ramsauer-Townsend minimum, behavior at the very-low-energy region does not alter very much.

In Fig. 4(a), the total-cross-section curve obtained by the MERT5+ fit, which is the MERT5 fit with an s-wave phase shift employing Eq. (13) instead of Eq. (2), is also shown. The solid curve representing the MERT5+ fit and the broken curve for the MERT5 fit agree well with each other in the energy region below 1.0 eV.

The MERT parameters obtained from the present analysis are shown in Tables II and III. Here we note that the uniqueness in determining the MERT parameters for p-wave and d-wave phase shifts is poor for the MERT6 fit to the total-cross-section data. In particular, the parameters A_1, H, and A_2 shown in Tables II and III include large uncertainties. On the other hand, the values of the scattering length (parameter A) are determined uniquely in the present fit to the experimental total-cross-section data. The values of the scattering length obtained in both the MERT5 fit and the MERT5+ fit for e^--Ar scattering are in good agreement. This also applies to the case

TABLE II. MERT parameters for electron scattering from Ar derived by MERT fits to the experimental total cross sections (in atomic units). The values used for α_d and α_q were 11.08 a_0^3 and 0.0 a_0^5, respectively [10,62]. The maximum energy used for each of the fits was 1.0 eV.

MERT parameters	Ar	
	(MERT5)	(MERT5+)
A	−1.370	−1.365
D	75.2	80.5
F	−116	−153
G		31.0
A_1	8.8	8.8
H	38.8	29.7

TABLE III. MERT parameters for electron scattering from Kr and Xe derived by the MERT fit to the experimental total cross sections (in atomic units). The values used for α_d and α_q were 16.74 a_0^3 and 8.0 a_0^5 for Kr, and 27.29 a_0^3 and 16.8 a_0^5 for Xe, respectively [62]. The maximum energy used for each of the fits was 1.0 eV.

MERT parameters	Kr		Xe	
	(MERT6)	(MERT6+)	(MERT6)	(MERT6+)
A	−3.11	−3.06	−5.56	−5.13
D	181	212	506	909
F	−264	−417	−805	−2336
G		109		1093
A_1	18.5	13.9	28.0	22.3
H	119	39.4	116	53.9
A_2	3.1	3.2	8.5	12.9

TABLE IV. Comparison of the scattering length obtained from the present MERT analysis with those obtained in previous studies [the quoted uncertainties in parentheses refer to the respective last digits].

	Scattering length (units of a_0)		
	Ar	Kr	Xe
Present work	−1.365(5)	−3.06(2)	−5.13(3)
Ferch *et al.* [7]	−1.449		
Buckman and Lohmann [8]	−1.492		
Buckman and Lohmann [9]		−3.19	
Buckman and Mitroy [10]	−1.442	−3.279	
Milloy *et al.* [16]	−1.50		
Haddad and O'Malley [59]	−1.488		
Hunter *et al.* [19]		−3.36	−6.09
England and Elford [18]		−3.43	
Mitroy [61]		−3.3873	
Brennan and Ness [21]		−3.3528	
Petrović *et al.* [23]	−1.459		

of e^--Kr scattering, where the discrepancy between the results for the MERT6 fit and the MERT6+ fit slightly increases compared to the case of e^--Ar scattering. In the case of e^--Xe, only the MERT6+ fit curve agrees with the experimental cross sections at very low energies, and the value of the scattering length obtained in the MERT6 fit differs from that obtained from the MERT6+ fit.

A comparison of the values of the scattering length obtained in the present MERT analysis with those reported in the previous studies is made in Table IV. As shown in Table IV, the present values of the scattering length obtained from the total cross sections measured in the extended energy range are smaller than the previous results in absolute value for each atom, especially for Xe. The scattering lengths obtained from beam measurements (Ferch *et al.* [7], Buckman and Lohmann [8,9], and Buckman and Mitroy [10]) may have uncertainty in extrapolating the cross-section curve down to zero energy by the MERT fit due to the restricted energy range of measurements ($E \leqslant \sim 0.1$ eV). On the other hand, although a very-low-electron-energy region, as low as 10 meV, is accessible in swarm experiments, deriving the momentum-transfer cross sections from the macroscopic experimental results includes a complicated and cumbersome unfolding procedure [22,24]. On the other hand, it is very straightforward and simple to obtain the absolute cross-section vales in the present method, and it was also shown that the present cross sections obtained above 100 meV show good agreement with the previous reliable beam experiments. Therefore, the scattering lengths reported here would be reliable compared to the previous ones.

C. Total cross sections for electron scattering from Ar, Kr, and Xe at around the Feshbach resonances

In the present study, we measured the total cross sections for electron scattering from Ar in the vicinity of the Ar^- $(3p^5 4s^2\,{}^2P_{3/2}, {}^2P_{1/2})$ Feshbach resonances with improved resolution and determined the resonance width. We also measured the total cross sections and analyzed the structure of the Kr^- $(4p^5 5s^2\,{}^2P_{3/2}, {}^2P_{1/2})$ Feshbach resonances and the Xe^- $(5p^5 6s^2\,{}^2P_{3/2}, {}^2P_{1/2})$ Feshbach resonances.

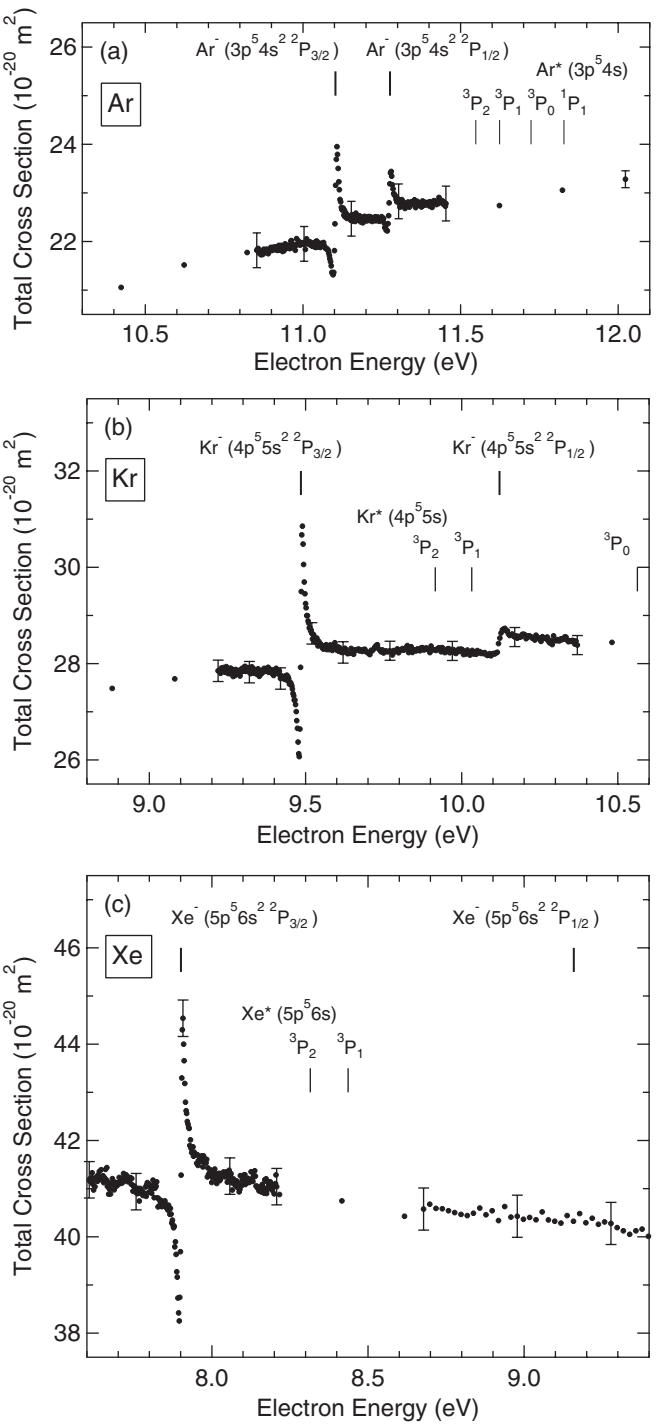

FIG. 5. Experimental total cross sections for electron scattering from Ar, Kr, and Xe at around the Feshbach resonances. (a) The Ar^- $(3p^5 4s^2\,{}^2P_{3/2}, {}^2P_{1/2})$ resonances. (b) The Kr^- $(4p^5 5s^2\,{}^2P_{3/2}, {}^2P_{1/2})$ resonances. (c) The Xe^- $(5p^5 6s^2\,{}^2P_{3/2}, {}^2P_{1/2})$ resonances. Vertical bars represent the energy position corresponding to the Feshbach resonances and the exited states of the neutral atom.

In Figs. 5(a)–5(c), total cross sections obtained at energies around the Feshbach resonances of Ar, Kr, and Xe are shown.

As can be seen in each of the figures, the narrow resonant structure due to the Feshbach resonances is clearly observed.

In Fig. 5(a), double sharp features due to the Ar^- $(3p^5 4s^2\,{}^2P_{3/2})$ resonance and the Ar^- $(3p^5 4s^2\,{}^2P_{1/2})$ resonance are seen. The intensity of the resonant structure of the $Ar^-\,{}^2P_{3/2}$ resonance is twice that of the $Ar^-\,{}^2P_{1/2}$ resonance, as was expected from the resonant theory within the framework of the potential scattering theory.

For Kr, the intensity of the structure due to the $Kr^-\,{}^2P_{1/2}$ resonance is smaller than that expected from the resonant scattering theory. In addition, the resonant width of the $Kr^-\,{}^2P_{1/2}$ resonance seems broader than that of the $Kr^-\,{}^2P_{3/2}$ resonance. These observations are explained by the fact that the $Kr^-\,{}^2P_{1/2}$ resonance appears above the energy of the first excited state of Kr $(4p^5 5s,\ J = 2)$ at 9.915 eV and the second excited state Kr $(4p^5 5s,\ J = 1)$ at 10.032 eV. Therefore, the $Kr^-\,{}^2P_{1/2}$ resonance can decay into both of these states in addition to the ground state. The scattering phase shifts for these inelastic channels would not be the same for those for the elastic channel, thus the lifetime of the $Kr^-\,{}^2P_{1/2}$ resonance would become shorter than that of the $Kr^-\,{}^2P_{3/2}$ resonance.

In Fig. 5(c), only the structure of the $Xe^-\,{}^2P_{3/2}$ resonance appeared clearly. In the case of Xe, we found that the structure due to the $Xe^-\,{}^2P_{1/2}$ resonance is very weak and could not be seen in the total cross sections within our experimental error. As was the case for the $Kr^-\,{}^2P_{1/2}$ resonance, the $Xe^-\,{}^2P_{1/2}$ resonance lies above the first two excited states of Xe, i.e., the Xe $(5p^5 6s,\ J = 2)$ state and the Xe $(5p^5 6s,\ J = 1)$ state. Since the structure due to the $Xe^-\,{}^2P_{1/2}$ resonance was observed very weakly in the previous elastic electron-scattering spectra [34], the present results of the faintness of the structure for the $Xe^-\,{}^2P_{1/2}$ resonance may be due to the destructive interference between the elastic and inelastic channels. The resonance width of the $Xe^-\,{}^2P_{1/2}$ resonance has been reported as 185 meV by Zubek *et al.* [34]. This value is significantly large relative to that of the $Xe^-\,{}^2P_{3/2}$ resonance, which has been reported as 3.6 to 4.5 meV previously [32,34,63].

D. The widths of the Feshbach resonances

The width of the resonance, which only decays into the elastic scattering channel, can be accurately determined through a standard partial-wave analysis. Here, we carried out the analysis of the resonance structure of the Ar^- $(3p^5 4s^2\,{}^2P_{3/2}$, ${}^2P_{1/2})$, the Kr^- $(4p^5 5s^2\,{}^2P_{3/2})$, and the Xe^- $(5p^5 6s^2\,{}^2P_{3/2})$ resonances. Analyses of the resonance structure were performed by fitting the model curve for the resonance structure, which was obtained from the partial-wave description for spin-dependent scattering convoluted with a Gaussian function of the width corresponding to the energy resolution of the experiment.

In the presence of significant spin-orbit coupling, the integral electron-scattering cross section for elastic scattering is given by

$$\sigma(E) = 2\pi \int_0^\pi \left(|f(\theta,E)|^2 + |g(\theta,E)|^2 \right) \sin\theta d\theta, \quad (14)$$

where the direct and exchange amplitude $f(\theta,E)$ and $g(\theta,E)$ are given by partial-wave sums as follows [64,65]:

$$f(\theta,E) = \frac{1}{2ik}\sum_l^\infty ((l+1)\{\exp[2i\delta_l^+(k)] - 1\} + l\{\exp[2i\delta_l^-(k)] - 1\})P_l(\cos\theta), \quad (15)$$

$$g(\theta,E) = \frac{1}{2ik}\sum_l^\infty \{\exp[2i\delta_l^+(k)] - \exp[2i\delta_l^-(k)]\}P_l^1(\cos\theta). \quad (16)$$

Here, k is the wave number of the electron related to the collision energy E, $P_l(\cos\theta)$ are the standard Legendre polynomials, $P_l^1(\cos\theta)$ $(L \geqslant 1)$ is an associated Legendre polynomial, while $\delta_l^+(k)$ and $\delta_l^-(k)$ represent the phase shifts in the partial wave with total electronic angular momenta of $j^+ = l + 1/2$ and $j^- = l - 1/2$, respectively. Rapid changes of the phase shift, $\delta_l^+(k)$ or $\delta_l^-(k)$, of the resonance partial wave ($l = 1$ for the present resonances) by a value of π cause the variation in the cross section. In the energy region close to a resonance at an energy E_r, the phase shift changes according to the expression

$$\delta_l^\pm(E) = \delta_l^{0\pm}(E) + \cot^{-1}\frac{E - E_r^\pm}{\Gamma^\pm/2}, \quad (17)$$

where Γ is the half width (natural width) of the resonance and $\delta_l^{0\pm}(E)$ is the potential (nonresonant) scattering phase shift, which varies only slowly with the electron energy. Therefore, the integral cross sections for elastic scattering close to the resonances become

$$\sigma(E) = \frac{\pi}{k^2}\left\{8\sin^2\left[\delta_1^{0+}(E) + \cot^{-1}\frac{E - E_{3/2}}{\Gamma_{3/2}/2}\right] + 4\sin^2\left[\delta_1^{0-}(E) + \cot^{-1}\frac{E - E_{1/2}}{\Gamma_{1/2}/2}\right]\right\} + \frac{\pi}{k^2}\sum_{l\neq 1}\left[4(l+1)\sin^2\delta_l^{0+}(E) + 4l\sin^2\delta_l^{0-}(E)\right]. \quad (18)$$

An accurate determination of the resonant width requires us to take into account the main factors that are likely to change the resonance shape, namely, finite resolving power due to electron-energy distribution and Doppler broadening in a static gas target, and also the effects of resonance amplification caused by high pressure in transmission measurements. By incorporating these factors into the attenuation method, the relation between $I(E)$ and $I_0(E)$ can be written as [30,66]

$$I(E) = I_0(E)\int\left\{G(E'' - E) \times \exp\left[-nL\int g(E' - E'')\sigma(E)dE'\right]\right\}dE'', \quad (19)$$

where $G(E'' - E)$ represents the energy distribution of the incident electrons around the nominal energy E, and $g(E' - E'')$ describes the broadening caused by the thermal motion of the target atom, i.e., Doppler broadening. The energy distribution of the incident electrons was assumed to be Gaussian with

a width at half intensity of w. The Doppler broadening can be represented by a one-dimensional form for the case of an electron-atom interaction as

$$g(E'-E'') = \frac{1}{\sqrt{4\pi ME/\mu kT}} \times \exp\left[-(\sqrt{E'}-\sqrt{E''})^2\frac{M}{\mu kT}\right], \tag{20}$$

where M is the mass of the target atom, μ is the reduced mass of the electron and the target atom, and k is the Boltzmann constant [67]. The cross section $\sigma^{\text{att}}(E)$ obtained with the attenuation law given by Eq. (1) is related to $\sigma(E)$ as follows:

$$\sigma^{\text{att}}(E) = -\frac{1}{nL}\ln\left(\int\left\{G(E''-E) \times \exp\left[-nL\int g(E'-E'')\sigma(E)dE'\right]\right\}dE''\right). \tag{21}$$

Here, let us introduce the cross section $\sigma_{\text{res}}(E)$ due to the resonant scattering and the cross section $\sigma_{\text{direct}}(E)$ due to direct scattering, and divide $\sigma(E)$ into resonant and nonresonant parts as

$$\sigma(E) = \sigma_{\text{res}}(E) + \sigma_{\text{direct}}(E). \tag{22}$$

The forms of $\sigma_{\text{res}}(E)$ and $\sigma_{\text{direct}}(E)$ are as follows:

$$\sigma_{\text{res}}(E) = \frac{8\pi}{k^2}\left[\sin^2\left(\delta_1^{0+} + \cot^{-1}\frac{E-E_{3/2}}{\Gamma_{3/2}/2}\right) - \sin^2\delta_1^{0+}\right] + \frac{4\pi}{k^2}\left[\sin^2\left(\delta_1^{0-} + \cot^{-1}\frac{E-E_{1/2}}{\Gamma_{1/2}/2}\right) - \sin^2\delta_1^{0-}\right], \tag{23}$$

$$\sigma_{\text{direct}}(E) = \frac{\pi}{k^2}\sum_l^{\infty}\left[4(l+1)\sin^2\delta_l^{0+} + 4l\sin^2\delta_l^{0-}\right]. \tag{24}$$

The nonresonant part in the observed section can be expressed as

$$\sigma^{\text{att}}_{\text{direct}}(E) = -\frac{1}{nL}\ln\left(\int\left\{G(E''-E) \times \exp\left[-nL\int g(E'-E'')\sigma_{\text{direct}}(E)dE'\right]\right\}dE''\right). \tag{25}$$

By substituting Eq. (22) into Eq. (21) and assuming $\sigma_{\text{direct}}(E)$ as a constant within the narrow energy range of the experimental width, the resonant cross section $\sigma^{\text{att}}_{\text{res}}(E)$ can be related to $\sigma_{\text{res}}(E)$ as follows, which would be a good approximation in the present case:

$$\sigma^{\text{att}}_{\text{res}}(E) = \sigma^{\text{att}}(E) - \sigma^{\text{att}}_{\text{direct}}(E) \sim -\frac{1}{nL}\ln\left(\int\left\{G(E''-E) \times \exp\left[-nL\int g(E'-E'')\sigma_{\text{res}}(E)dE'\right]\right\}dE''\right). \tag{26}$$

TABLE V. Nonresonant phase shifts for $l = 1$ partial waves employed in the present analysis.

	$\delta_1^{0\pm}(E)$ (rad)	E (eV)	Reference
Ar	−0.5916	11.00	Franz *et al.* [35]
	−0.6062	11.36	
Kr	−0.657	9.0	Bell *et al.* [68]
	−0.717	10.0	
Xe	−0.707	7.5	Heindorff *et al.* [63]

Equation (26) was fitted to the experimentally observed resonant cross section $\sigma^{\text{exp}}_{\text{res}}(E)$ with the resonance width Γ and the width corresponding to the energy resolution of the electron beam w, which is related to the function $G(E''-E)$ as the fitting parameters. No scaling factor for the intensity was employed in the fit. In the present form, only the nonresonant phase shifts for $l = 1$ partial waves are required for the fit.

In the present study, $\sigma^{\text{exp}}_{\text{res}}(E)$ was obtained by subtracting $\sigma^{\text{exp}}_{\text{direct}}(E)$ approximated with a third-order polynomial from the measured cross-section curve. The nonresonant phase shifts for $l = 1$ partial waves were chosen as shown in Table V, which gives the best fit to our experimental results. For Ar and Kr, phase shifts at energies between the reported energies were obtained from interpolation of the values of Table V. In the case of Xe, a satisfactory fit was made by using the phase shift of Heindorff *et al.*, obtained at 7.5 eV [63].

In Fig. 6, $\sigma^{\text{exp}}_{\text{res}}(E)$ together with the fitted curves $\sigma^{\text{att}}_{\text{res}}(E)$ obtained from Eq. (26) are shown. Each of the fitted curves reproduces the experimental cross sections very well. The energy widths of the electron beam, w, were 8.4, 7.0, and 8.6 meV for the measurements of Ar, Kr, and Xe, respectively. The results of the resonance widths obtained in the present analysis are shown in Table VI together with those of previous experimental work.

The present results for the resonance widths for the $Ar^-\ ^2P_{3/2}$ and the $Ar^-\ ^2P_{1/2}$ resonances show very good agreement with those by Dubé *et al.* [32] and Franz *et al.* [35]. The recent value of Franz *et al.* was based on a phase-shift analysis of the absolute angle differential cross sections measured with two different experimental setups. One was the electron-scattering apparatus with a very-high-energy resolution of 5 meV employing the laser photoelectron source at Kaiserslautern. The other was the high-resolution electron-scattering apparatus with resolution of 13 meV combined with a magnetic angle changer at Fribourg. By assuming that both the $Ar^-\ ^2P_{3/2}$ and $^2P_{1/2}$ resonances have identical widths, they obtained the resonance widths of 2.3 meV for the Ar^- resonances, which seem to be the most accurate value in the previous work. They also noted that allowing for nonidentical values of the width for the $^2P_{3/2}$ and $^2P_{1/2}$ resonances in their fit gives the results of $\Gamma_{3/2} \leqslant \Gamma_{1/2} + 0.1$ meV, which gives the excellent agreement with the present results for the $Ar^-\ ^2P_{3/2}$ and $^2P_{1/2}$ resonances.

For Kr, the present width of the $Kr^-\ ^2P_{3/2}$ resonance is somewhat narrow compared to those obtained in the previous experiments, as shown in Table VI. The experimental value of Hoffmann *et al.* [36] was obtained by the phase-shift analysis of the absolute angle differential cross sections measured with

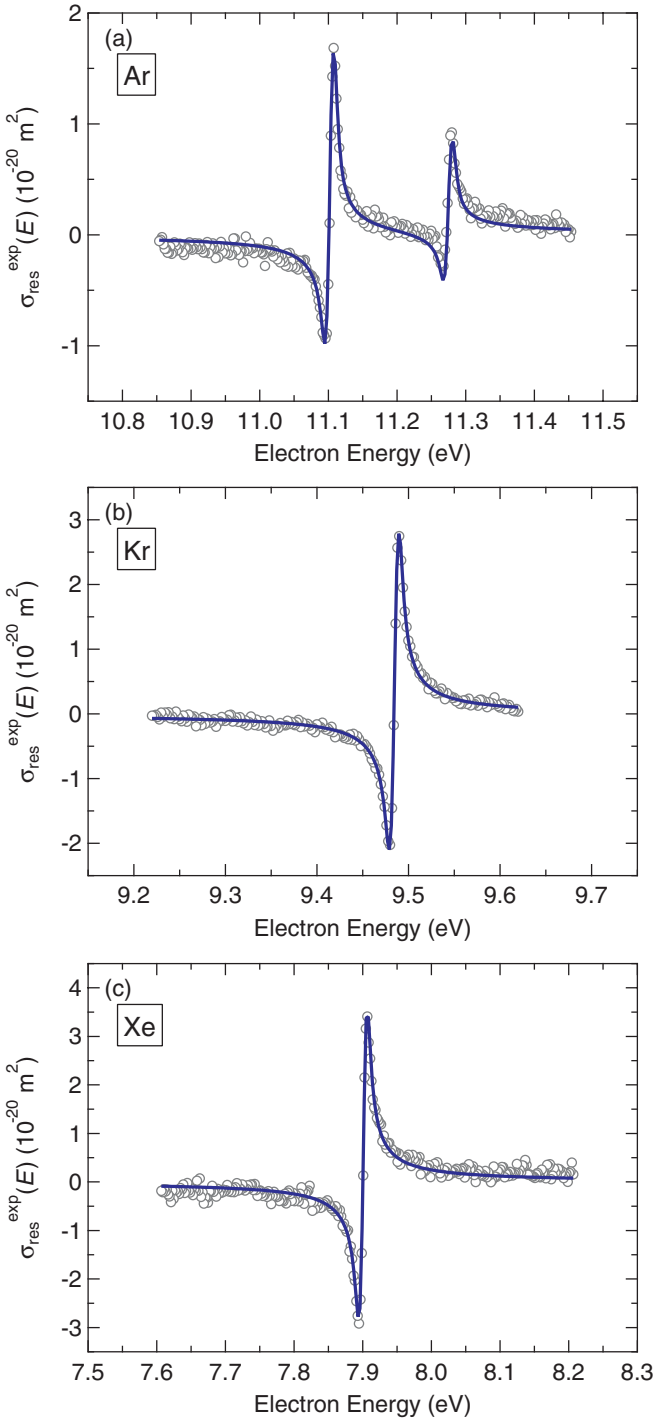

FIG. 6. (Color online) Profiles of the cross sections due to the Feshbach resonances, $\sigma_{res}^{exp}(E)$ (open circles), and the best fits for the resonant cross sections obtained by fitting the calculated $\sigma_{res}^{att}(E)$ (solid curves); (a) the Ar^- $(3p^5 4s^2\,{}^2P_{3/2})$ and the Ar^- $(3p^5 4s^2\,{}^2P_{1/2})$ resonances, (b) the Kr^- $(4p^5 5s^2\,{}^2P_{3/2})$ resonance, and (c) the Xe^- $(5p^5 6s^2\,{}^2P_{3/2})$ resonance.

the Fribroug instrument used in the work of Franz *et al.* [35]. In the case of Kr, the present results did not agree with the value obtained by the high-resolution measurements of Hoffmann *et al.* The disagreement seems to be the result of using the different phase shifts in the analysis of each study. In the present study, the phase shift of Bell *et al.* [68] was used for the nonresonant part of the $l = 1$ partial wave. We chose the phase shift of Bell *et al.* not only because their integral cross-section curve agrees well with our recent experimental results for Kr at around the resonance energy [25], but also because their phase shift gave the best fit in the present analysis. Four sets of the phase shifts have been employed in the analysis of Hoffmann *et al.* and their results, shown in Table VI, are the weighted mean of each fit. They also reported the value of 3.31 meV for the results of using the phase shift of Bell *et al.* [68], which agrees very well with the present value.

TABLE VI. Comparison of the resonance widths Γ of the Ar^- $(3p^5 4s^2\,{}^2P_{3/2})$ and the Ar^- $(3p^5 4s^2\,{}^2P_{1/2})$ resonances, the Kr^- $(4p^5 5s^2\,{}^2P_{3/2})$ resonance, and the Xe^- $(5p^5 6s^2\,{}^2P_{3/2})$ resonance.

	Reference	$\Gamma\ ({}^2P_{3/2})$	$\Gamma\ ({}^2P_{1/2})$
Ar			
	Weingartshofer *et al.* (1974) [69]	3–4	
	Brunt *et al.* (1977) [70]	2.5 ± 0.5	
	Dubé *et al.* (1993) [32]	2.3 ± 0.2	
	Hammond (1996) [33]	3.4 ± 0.2	3.2 ± 0.2
	Franz *et al.* (2008) [35]	2.3 ± 0.2	
	Present work	2.3 ± 0.2	2.2 ± 0.4
Kr			
	Swanson *et al.* (1973) [31]	3.8–6	
	Weingartshofer *et al.* (1974) [69]	8	
	Dubé *et al.* (1993) [32]	3.6 ± 0.4	
	Zubek *et al.* (1999) [34]	3.5 ± 1.0	30 ± 4
	Hoffmann *et al.* (2010) [36]	3.6 ± 0.2	33 ± 5
	Present work	3.2 ± 0.1	
Xe			
	Heindorff *et al.* (1976) [63]	4.5 ± 1.0	
	Dubé *et al.* (1993) [32]	3.6 ± 1.0	
	Zubek *et al.* (1999) [34]	4.0 ± 1.0	185 ± 20
	Present work	4.1 ± 0.2	

In the case of Xe, the width of the $Xe^-\ {}^2P_{3/2}$ resonance was obtained with much higher precision compared to the previous reports. The present results agree well with the previous results, especially for those by Zubek [34].

The reliable absolute value of the present cross sections, which can be obtained more precisely in the total-cross-section measurements compared to the differential cross-section measurements, enables us to determine Γ and w uniquely without any scaling factor in the fit. It is also noted that the present analysis also has an advantage that the fit can be easily carried out without suffering from choosing the reliable phase shifts for nonresonant partial waves.

IV. CONCLUSIONS

The absolute total cross sections for electron scattering from Ar and Xe were obtained in the energy range from 20 eV down to 7 meV, with very narrow electron-energy widths of 10–12 meV using the threshold-photoelectron source. Total cross sections obtained in the present study generally agree well with those obtained in the previous experiments [7,8, 46,52–54,57] above 100 meV, including the position and the

magnitude of the Ramsauer- Townsend minimum, except for the values reported by Gus'kov *et al.* [6] at the very-low-energy region.

Scattering lengths for e^--Ar, -Kr, and -Xe scattering were determined using the modified effective range theory. The values were -1.365, -3.06, and -5.13 a_0 for Ar, Kr, and Xe, respectively. It was found that the scattering lengths for these rare-gas atoms obtained in the previous studies [7–10,16,18,19,21,23,59,61] show larger absolute values compared to the present values due to the overestimation of the cross sections at very low energies below 100 meV, where direct measurements in the single-collision condition have not been reported.

The total cross sections at around the Ar^- ($3p^5 4s^2\,{}^2P_{3/2}$, ${}^2P_{1/2}$), Kr^- ($4p^5 5s^2\,{}^2P_{3/2}$, ${}^2P_{1/2}$), and Xe^- ($5p^5 6s^2\,{}^2P_{3/2}$, ${}^2P_{1/2}$) resonances were also studied, with improved energy resolution. The widths of the Ar^- ($3p^5 4s^2\,{}^2P_{3/2}$ and ${}^2P_{1/2}$) resonances obtained from the partial-wave analysis to the present total cross sections were 2.3 ± 0.2 and 2.2 ± 0.4 meV, respectively, which agree very well with those obtained by recent studies based on the differential cross section at very high resolution [35]. Widths of the Kr^- ($4p^5 5s^2\,{}^2P_{3/2}$) and Xe^- ($5p^5 6s^2\,{}^2P_{3/2}$) resonances were also determined precisely as 3.2 ± 0.1 and 4.1 ± 0.2 meV, respectively. The analysis based on the partial-wave analysis to the high-resolution total-cross-section measurements was shown to be a powerful method for the accurate determination of the resonance widths.

ACKNOWLEDGMENTS

This work was supported by the Grant-in-Aid for Scientific Research (C) (Grants No. 18540390 and No. 20540387) of the Japan Society for the Promotion of Science, and a Cooperative Research Grant from the National Institute for Fusion Science, Japan (Grant No. NIFS06KYAM010). This work has been carried out under the approval of the Photon Factory Program Advisory Committee for Proposals No. 2008G639 and No. 2010G603.

[1] C. Ramsauer, Ann. Phys. (Leipzig) **66**, 546 (1922).
[2] J. S. Townsend and V. A. Bailey, Philos. Mag. **43**, 593 (1922).
[3] T. F. O'Malley, Phys. Rev. **130**, 1020 (1963).
[4] D. E. Golden and H. W. Bandel, Phys. Rev. **149**, 58 (1966).
[5] D. E. Golden, Phys. Rev. **151**, 48 (1966).
[6] Yu. K. Gus'kov, R. V. Savvov, and V. A. Slobodyanyuk, Sov. Phys.-Tech. Phys. **23**, 167 (1978).
[7] J. Ferch, B. Granitza, C. Masche, and W. Raith, J. Phys. B **18**, 967 (1985).
[8] S. J. Buckman and B. Lohmann, J. Phys. B **19**, 2547 (1986).
[9] S. J. Buckman and B. Lohmann, J. Phys. B **20**, 5807 (1987).
[10] S. J. Buckman and J. Mitroy, J. Phys. B **22**, 1365 (1989).
[11] A. C. Gallagher and G. York, Rev. Sci. Instrum. **45**, 662 (1974).
[12] R. E. Kennerly, R. J. VanBrunt, and A. C. Gallagher, Phys. Rev. A **23**, 2430 (1981).
[13] D. Field, S. L. Lunt, and J.-P. Ziesel, Acc. Chem. Res. **34**, 291 (2001).
[14] S. V. Hoffmann, S. L. Lunt, N. C. Jones, D. Field, and J.-P. Ziesel, Rev. Sci. Instrum. **73**, 4157 (2002).
[15] L. S. Frost and A. V. Phelps, Phys. Rev. **136**, A1538 (1964).
[16] H. B. Milloy, R. W. Maeda, J. A. Rees, and A. G. Robertson, Aust. J. Phys. **30**, 61 (1977).
[17] T. Koizumi, E. Shirakawa, and I. Ogawa, J. Phys. B **19**, 2331 (1986).
[18] J. P. England and M. T. Elford, Aust. J. Phys. **41**, 701 (1988).
[19] S. R. Hunter, J. G. Carter, and L. G. Christophorou, Phys. Rev. A **38**, 5539 (1988).
[20] J. L. Pack, R. E. Voshall, A. V. Phelps, and L. E. Kline, J. Appl. Phys. **71**, 5363 (1992).
[21] M. J. Brennan and K. F. Ness, Aust. J. Phys. **46**, 249 (1993).
[22] B. Schmidt, K. Berkhan, B. Götz, and M. Müller, Phys. Scr. T **53**, 30 (1994).
[23] A. L. Petrović, T. F. O'Malley, and R. W. Crompton, J. Phys. B **28**, 3309 (1995).
[24] A. L. Petrović, S. Dujko, D. Marić, G. Malović, Ž. Nikitović, O. Šašić, J. Jovanović, V. Stojanović, and M. Radmilović-Radenović, J. Phys. D **42**, 194002 (2009).
[25] M. Kurokawa, M. Kitajima, K. Toyoshima, T. Odagiri, H. Kato, H. Kawahara, M. Hoshino, H. Tanaka, and K. Ito, Phys. Rev. A **82**, 062707 (2010).
[26] T. F. O'Malley, L. Rosenberg, and L. Spruch, Phys. Rev. **125**, 1300 (1962).
[27] T. F. O'Malley and R. W. Crompton, J. Phys. B **13**, 3451 (1980).
[28] G. J. Schulz, Phys. Rev. **136**, A650 (1964).
[29] L. Sanche and G. J. Schulz, Phys. Rev. A **5**, 1672 (1972).
[30] C. E. Kuyatt, J. A. Simpson, and S. R. Mielczarek, Phys. Rev. **138**, A385 (1965).
[31] N. Swanson, J. W. Cooper, and C. E. Kuyatt, Phys. Rev. A **8**, 1825 (1973).
[32] D. Dubé, D. Tremblay, and D. Roy, Phys. Rev. A **47**, 2893 (1993).
[33] P. Hammond, J. Phys. B **29**, L231 (1996).
[34] M. Zubek, B. Mielewska, J. Channing, G. C. King, and F. H. Read, J. Phys. B **32**, 1351 (1999).
[35] K. Franz, T. H. Hoffmann, J. Bömmels, A. Gopalan, G. Sauter, W. Meyer, M. Allan, M.-W. Ruf, and H. Hotop, Phys. Rev. A **78**, 012712 (2008).
[36] T. H. Hoffmann, M.-W. Ruf, H. Hotop, O. Zatsarinny, K. Bartschat, and M. Allan, J. Phys. B **43**, 085206 (2010).
[37] K. Ito, Y. Morioka, M. Ukai, N. Kouchi, Y. Hatano, and T. Hayaishi, Rev. Sci. Instrum. **66**, 2119 (1995).
[38] S. Cvejanović and F. H. Read, J. Phys. B **7**, 1180 (1974).
[39] W. F. Chan, G. Cooper, and C. E. Brion, Phys. Rev. A **44**, 186 (1991).
[40] T. Takaisi and Y. Sensui, Trans. Faraday Soc. **59**, 2503 (1963).
[41] CPO, Ltd., computer code CPO (Charged Particle Optics programs) [http://www.electronoptics.com].
[42] R. P. McEachran and A. D. Stauffer, J. Phys. B **16**, 4023 (1983).
[43] R. P. McEachran and A. D. Stauffer, J. Phys. B **17**, 2507 (1984).
[44] H. Takaki, N. Nakamura, Y. Kobayashi, K. Harada, T. Miyajima, A. Ueda, S. Nagahashi, M. Shimada, T. Obina, and T. Honda, Phys. Rev. ST Accel. Beams **13**, 020705 (2010).

[45] J. C. Nickel, K. Imre, D. F. Register, L. Vuskovic, and S. Trajmar, J. Phys. B **18**, 125 (1985).
[46] K. Jost, P. G. F. Bisling, F. Eschen, M. Felsmann, and L. Walther, in *Abstracts of Contributed Papers, 13th International Conference on the Physics of Electronic and Atomic Collisions, Berlin, 1983*, edited by J. Eichler, W. Fritsch, I. V. Hertel, N. Stolterfoht, and U. Wille (Berlin, Germany, 1983), p. 91.
[47] K. L. Bell, N. S. Scott, and M. A. Lennon, J. Phys. B **17**, 4757 (1984).
[48] J. Yuan, J. Phys. B **21**, 3753 (1988).
[49] B. Plenkiewicz, P. Plenkiewicz, and J. P. Jay-Gerin, Phys. Rev. A **38**, 4460 (1988).
[50] D. J. R. Mimnagh, R. P. McEachran, and A. D. Stauffer, J. Phys. B **26**, 1727 (1993).
[51] R. P. McEachran and A. D. Stauffer, Aust. J. Phys. **50**, 511 (1997).
[52] K. P. Subramanian and V. Kumar, J. Phys. B **20**, 5505 (1987).
[53] C. Szmytkowski, K. Maciąg, and G. Karwasz, Phys. Scr. **54**, 271 (1996).
[54] J. Ferch, F. Simon, and G. Strakeljahn, in *Abstracts of Contributed Papers, 15th International Conference on the Physics of Electronic and Atomic Collisions, Brighton, 1987*, edited by J. Geddes, H. B. Gilbody, A. E. Kingston, C. J. Latimer, and H. J. R. Walters (Brighton, UK, 1987), p. 132.
[55] R. P. McEachran and A. D. Stauffer, J. Phys. B **20**, 3483 (1987).
[56] J. E. Sienkiewicz and W. E. Baylis, J. Phys. B **22**, 3733 (1989).
[57] D. T. Alle, M. J. Brennan, and S. J. Buckman, in *Abstracts of Contributed Papers, 18th International Conference on the Physics of Electronic and Atomic Collisions, Aarhus, 1993*, edited by T. Andersen, B. Fastrup, F. Folkmann, and H. Knudsen (Aarhus, Denmark, 1993), p. 127.
[58] J. Yuan and Z. Zhang, J. Phys. B **24**, 275 (1991).
[59] G. N. Haddad and T. F. O'Malley, Aust. J. Phys. **35**, 35 (1982).
[60] M. Weyhreter, B. Barzick, A. Mann, and F. Linder, Z. Phys. D **7**, 333 (1988).
[61] J. Mitroy, Aust. J. Phys. **43**, 19 (1990).
[62] A. Dalgarno and A. E. Kingston, Proc. R. Soc. A **259**, 424 (1960).
[63] T. Heindorff, J. Hofft, and P. Dabkiewicz, J. Phys. B **9**, 89 (1976).
[64] N. F. Mott and H. S. W. Massey, *The Theory of Atomic Collisions* (Oxford University Press, Oxford, 1965).
[65] J. Bömmels, K. Franz, T. H. Höffmann, A. Gopalan, O. Zatsarinny, K. Bartschat, M.-W. Ruf, and H. Hotop, Phys. Rev. A **71**, 012704 (2005).
[66] D. Roy, A. Delage, and J.-D. Carette, J. Phys. E **8**, 109 (1984).
[67] P. J. Chantry, J. Chem. Phys. **55**, 2746 (1971).
[68] K. L. Bell, K. A. Berrington, and A. Hibbert, J. Phys. B **21**, 4205 (1988).
[69] A. Weingartshofer, K. Willmann, and E. M. Clarke, J. Phys. B **7**, 79 (1974).
[70] J. N. H. Brunt, G. C. King, and F. H. Read, J. Phys. B **10**, 1289 (1977).